

AIAA 2000-4876

**MULTI-OBJECTIVE OPTIMIZATION OF
TURBOMACHINERY CASCADES FOR
MINIMUM LOSS, MAXIMUM LOADING, AND
MAXIMUM GAP-TO-CHORD RATIO**

B. H. Dennis
The Pennsylvania State University
University Park, Pennsylvania

I. N. Egorov
Keldysh Institute of Applied Mathematics
Moscow, Russia

Z.-X. Han and G. S. Dulikravich
The University of Texas at Arlington
Arlington, Texas

C. Poloni
Universita di Trieste
Trieste, Italy

**8th AIAA/NASA/USAF/ISSMO Symposium on
Multidisciplinary Analysis and Optimization**
6-8 September 2000
Long Beach, California

MULTI-OBJECTIVE OPTIMIZATION OF TURBOMACHINERY CASCADES FOR MINIMUM LOSS, MAXIMUM LOADING, AND MAXIMUM GAP-TO-CHORD RATIO

Brian H. Dennis¹

Department of Aerospace Engineering, 233 Hammond
The Pennsylvania State University
University Park, PA 16802, U.S.A.

Igor N. Egorov²

Keldysh Institute of Applied Mathematics
Milashenkova 10-201
Moscow 127322, RUSSIA

Zhen-Xue Han³

Department of Mechanical and
Aerospace Engineering, Box 19018
The University of Texas at Arlington
Arlington, TX 76019, U.S.A.

George S. Dulikravich⁴

Department of Mechanical and Aerospace
Engineering, Box 19018
The University of Texas at Arlington
Arlington, TX 76019, U.S.A.

Carlo Poloni⁵

Dipartimento di Energetica
Universita' di Trieste
Via Valerio 10,
34127 Trieste, ITALY

Abstract

This paper illustrates an automatic multi-objective design optimization of a two-dimensional airfoil cascade row having a finite number of airfoils. The objectives were to simultaneously minimize the total pressure loss, maximize total aerodynamic loading (force tangent to the cascade), and minimize the number of airfoils in the finite cascade row. The constraints were: fixed mass flow rate, fixed axial chord, fixed inlet and exit flow angles, fixed blade cross-section area, minimum allowable thickness distribution, minimum allowable lift force, and a minimum allowable trailing edge radius. This means that the entire airfoil cascade shape was optimized including its stagger angle, thickness, curvature, and solidity. The analysis of the performance of intermediate airfoil cascade shapes were performed using an unstructured grid based compressible Navier-Stokes flow-field analysis code with $k-\epsilon$ turbulence model. A robust stochastic algorithm was used in the automatic multi-objective constrained shape design process that had 18 design variables, 5 nonlinear constraints, and 3 objectives. Simultaneous reductions of the total pressure loss, increases of the total loading, and decreases of the number of airfoils were achieved using this method on a VKI high subsonic exit flow axial turbine cascade.

I. Introduction

The attention of design engineers has been rapidly shifting from the use of repetitive computational analysis, personal experience, and intuition towards a reliable and economical mathematically based optimization algorithms. This trend has exposed the substantial weakness of traditional gradient based optimization approaches that easily terminate in a local minimum, can usually produce only single-objective optimized solutions, and require that the objective function satisfies continuity and derivability conditions. These facts, together with the growing need for multi-disciplinary and multi-objective approach to design with a large number of design variables, resulted in an increased interest in the use of various versions of stochastic optimization algorithms.

Examples of *single*-objective constrained airfoil cascade shape optimization were published recently demonstrating the feasibility of using various genetic algorithms in conjunction with Euler equations solvers¹⁻⁴ and Navier-Stokes flow-field analysis codes^{5,6}. These were examples of constrained optimization of a *single* objective (minimization of total pressure loss) while keeping the gap-to-chord ratio (cascade solidity) fixed.

A typical *multiple* objective of a design for retrofit of an existing cascade would be to fix the number of airfoils and total loading (specific work) of a finite cascade (sum of lift forces generated by all of the airfoils in a finite cascade) while minimizing the total pressure loss across the cascade. This approach represents a natural next step that could follow design optimization for a retrofit of a multistage turbomachine^{7,8} where optimized inlet and exit flow angles were *a priori* determined for each blade row.

¹ Graduate Research Assistant. Student member AIAA.

² Professor. Member of Russian Academy of Sciences.

³ Visiting Research Associate.

⁴ Professor. Director of MAIDO Laboratory. Associate Fellow AIAA.

⁵ Associate Professor.

A considerably more challenging problem is to simultaneously maximize the loading on the entire finite cascade, minimize the total pressure loss across the cascade, and minimize the total number of airfoils in the finite cascade. For the fixed mass flow rate and inlet and exit flow-field conditions this means maximizing gap-to-chord ratio (minimizing solidity) of the cascade simultaneously with the optimization of the airfoil shape. Reduction of the number of blades reduces the capital costs and the life cost of the turbomachine.

Therefore, results of such multi-objective constrained optimization should give the designer more options when making a final decision which of the feasible optimized cascades is the best.

It should be pointed out that including more objectives in the optimization process often has similar effects on the overall optimization effort required as including more constraints especially if these constraints are incorporated as penalty functions.

II. Multi-Objective Stochastic Optimizer

The *multi-objective* optimization problem can be expressed as follows. Maximize a vector of n objective functions

$$\max F_i(\bar{X}) \quad \text{for } i = 1, \dots, n \quad (1)$$

subject to a vector of inequality constraints

$$g_j(\bar{X}) \leq 0 \quad \text{for } j = 1, \dots, m \quad (2)$$

and a vector of equality constraints

$$h_q(\bar{X}) = 0 \quad \text{for } q = 1, \dots, k \quad (3)$$

In general, the solution of this problem is not unique. With the introduction of the Pareto dominance concept the possible solutions are divided in two subgroups: the *dominated* and the *non-dominated*. The solutions belonging to the second group are the "efficient" solutions, that is, the ones for which it is not possible to increase any objective without deteriorating the values of the remaining objectives. In formal terms, in case of a maximization problem, it is possible to write that the solution \bar{X} dominates the solution \bar{Y} if the following relation is true:

$$\bar{X} >_p \bar{Y} \Leftrightarrow (\forall i F_i(\bar{X}) \geq F_i(\bar{Y})) \cap (\exists j: F_j(\bar{X}) > F_j(\bar{Y})) \quad (4)$$

Classical gradient based optimization algorithms are capable, under strict continuity and derivability hypotheses, of finding the optimal value only in the case of a single objective. Therefore, the problem of finding the group of non-dominated solutions (the

Pareto front) is reduced to several single objective optimizations where the objective becomes a weighted combination of the objectives called utility function, U .

$$U(\bar{X}) = \sum_{i=1}^n W_i \cdot F_i(\bar{X}) \quad (5)$$

Recently, *multi-objective* optimization algorithms based on a genetic algorithm have been successfully applied in aerodynamic shape design^{9,10}. But, for a very large number of design variables and especially for a very large number of objective functions that need to be extremized simultaneously, this approach becomes progressively too costly. An alternative for such problems is a novel stochastic optimization formulation combined with a response surface approach.

The *multi-objective* constrained optimization algorithm used in this work is the modified version of an indirect method of optimization based upon self-organization (IOSO) and evolutionary simulation principles^{11,12}. Each iteration of IOSO consists of two steps. First step is creation of an approximation of the objective function(s). Each iteration in this step represents a decomposition of initial approximation function into a set of simple approximation functions. The final response function is a multilevel graph. Second step is the optimization of this approximation function. This approach allows for corrections of the structure and the parameters of the response surface approximation. The distinctive feature of this approach is an extremely low number of trial points to initialize the algorithm (30-50 points for the optimization problems with nearly 100 design variables).

The obtained response functions are used in the procedures of multilevel optimization with the adaptive changing of the simulation level within the frameworks of both single and multiple disciplines of the object analysis. In the process of each iteration of IOSO work the optimization of the response function is carried out within current search area. This step is followed by the direct call to the mathematical model for the obtained point. During the IOSO work the information concerning the behavior of the objective function nearby the extremum is stored, and the response function is made more accurate just for this search area. While passing from one iteration to another, following steps are carried out: the modification of the experiment plan; the adaptive selection of current extremum search area; the choice of the response function type (global or middle-range); the transformation of the response function; the modification of both parameters and structure of the optimization algorithms; and, if necessary, the selection of new promising points within the researched area.

Thus, during each iteration a series of approximation functions for particular criteria of optimization is built. These functions differ from each other according to both structure and definition range. The subsequent

optimization of the given approximation functions allows us to determine a set of vectors of optimized variables, which are used for computation of optimization criteria on a parallel computer.

III. Geometry Parameterization

During the cascade shape optimization process, flow-fields for a large number of different cascade airfoil geometries need to be analyzed. The airfoil shape was defined with the following nine parameters: the tangential and axial chord, the inlet and exit half wedge angle, the inlet and outlet airfoil angle, the throat, unguided turning angle, and the leading and trailing edge radii¹¹. One of these parameters (axial chord) was kept fixed. The airfoil shape was allowed significant additional flexibility by adding a continuous arbitrary perturbation in addition to the original nine parameters. This shape perturbation was modeled with a B-spline that had eight control vertices thus resulting in a total of $9 + 8 = 17$ design variables⁶ plus one additional variable for the number of airfoils in a finite length cascade. The design variables' ranges were set so that the optimizer would have a wide variety of very different airfoil shapes so as to test its robustness.

IV. Viscous Flow-Field Analysis Code

For the aerodynamic analysis of the performance of each candidate airfoil cascade we used two-dimensional Reynolds averaged compressible Navier-Stokes equations in conjunction with standard k- ϵ equations turbulence model¹⁴. The equations were discretized using finite volume scheme. Considering the significant shape variations of the airfoil cascade during current multi-objective optimization, unstructured triangular grid elements were used (Fig. 1) to automatically discretize the computational domain and cluster the grid points in the vicinity of the airfoil surface and wake region¹⁵. The discretized Navier-Stokes equations fully coupled with the turbulence model equations were integrated in time using an explicit four-stage Runge-Kutta time-stepping scheme¹⁶. Local time stepping and pseudo-Laplacian residual smoothing techniques were used to accelerate the convergence to steady state solution^{17,18}. The convective fluxes were computed using the Roe flux-difference splitting approach¹⁹, while the viscous fluxes were calculated with central difference scheme. Accuracy of the flow-field analysis code can be evaluated by comparing computed and experimentally measured surface isentropic Mach number distribution (Fig. 2) on an axial turbine cascade tested²⁰ by the VKI. Figure 3 also demonstrates the calculated field of iso-Mach contours.

V. Test Problem Definition

As an example of a realistic initial airfoil cascade on which the multi-objective constrained optimization will be performed, we chose to use the VKI cascade²⁰. It should be pointed out that this cascade had already a very high efficiency because it was designed using an inverse shape design method. Using inlet and exit boundary conditions and the geometry of this initial airfoil cascade, we assumed an annular stator finite cascade with the following conditions:

inlet total temperature $T_{01} = 278$ K
 inlet total pressure $p_{01} = 430000$ Pa
 exit average static pressure $p_2 = 101300$ Pa
 inlet flow angle = 1.9 degrees
 span radius = 223.8 mm
 number of airfoils = 45

The exit flow angle can be optimized *a priori* using a very efficient multistage optimization algorithm^{7,8}. Using our two-dimensional linear cascade Navier-Stokes flow-field analysis code, the following flow-field parameters were predicted for this annular stator finite cascade:

loading force (for 45 airfoils) = 186599 N
 mass-flow-averaged total pressure loss = 103078 Pa
 mass flow rate (for 45 passages) per unit span = $384 \text{ kg m}^{-1} \text{ s}^{-1}$
 exit flow angle = -70°
 single airfoil cross-section area = 108.8 mm^2

With these conditions we defined the following objectives (Table 1) and the constraints (Table 2).

Table 1. Simultaneous objectives in the multi-objective constrained optimization

	OBJECTIVES
MAXIMIZE	Total loading force
MINIMIZE	Total pressure loss
MINIMIZE	Number of airfoils

Table 2. Inequality and equality constraints used in the multi-objective constrained optimization

CONSTRAINTS	Values
Total loading	> 186599 N
Mass flow rate (per unit span)	$= 384 \text{ kg m}^{-1} \text{ s}^{-1}$
Exit flow angle	$= -70^\circ$
Airfoil cross-section area	$= 108.8 \text{ mm}^2$
Airfoil trailing edge radius	$= 0.5$ mm

The constraints were incorporated in the objective functions via penalty formulation. For this problem, the following objective functions are to be minimized simultaneously.

$$F_1 = p_o^{outlet} - p_o^{inlet} + c_1 \left(\frac{-70.0 - \theta}{-70.0} \right)^2 + c_2 \left(\frac{384.0 - \dot{m}}{384.0} \right)^2 + c_3 \left(\frac{0.0001088 - A}{0.0001088} \right)^2 + c_4 \left(\frac{186599 - L}{L} \right)^2 + c_5 (td)^2 \quad (6)$$

$$F_2 = -L + c_1 \left(\frac{-70.0 - \theta}{-70.0} \right)^2 + c_2 \left(\frac{384.0 - \dot{m}}{384.0} \right)^2 + c_3 \left(\frac{0.0001088 - A}{0.0001088} \right)^2 + c_4 \left(\frac{186599 - L}{L} \right)^2 + c_5 (td)^2 \quad (7)$$

$$F_3 = nb \quad (8)$$

Here, p_0 is the total pressure, θ is the average exit flow angle, \dot{m} is the mass flow rate, A is the cross-sectional area of the airfoil, nb is the total number of airfoils, and L is the total loading. The variable td is the largest relative error in the airfoil thickness distribution compared to a specified minimum allowable thickness distribution. This geometric constraint prevents airfoil from becoming too thin, thus mechanically or thermally infeasible. The constants c_i are user specified penalty terms. For this application, the penalty constants were initially set to 100000. A value of zero was used for the constants when any of the constraints were within one percent above or below the target constraint value.

VI. Numerical Results

With these definitions we performed a constrained multi-objective shape optimization of the finite VKI cascade. That is, we were able to observe if our optimization creates improved and realistic results since we were able to compare them with a realistic initial finite cascade configuration. For this constrained multi-objective optimization we used a modified IOSO.

In a multi-objective optimization we strive to compute the group of the *not-dominated* solutions which is known as a Pareto front. These are the feasible solutions found during the optimization that cannot be improved for one objective without sacrificing another. In Figs. 4-6 it is possible to see the points that belong to two-dimensional projections of the actual three-dimensional Pareto surface demonstrating that the multi-objective optimization was successful. One can also see that there was a design that was better than the original VKI airfoil for all three objectives. Thus the VKI airfoil is not a member of the final Pareto optimal set. In the Pareto front we chose to compare three optimized solutions (cascades No.1, No.3, and No.6 in Table 3). These are some of the best feasible solutions obtained during the constrained multi-objective optimization.

Table 3. A comparison of the three objectives achieved by the original VKI cascade and the three prominent cascades obtained with our multi-objective constrained optimization.

	VKI	No.1	No.3	No.6
Total pressure loss, Pa	103078	95164	97050	95012
Number of airfoils	45	44	46	45
Total loading, N	186599	189359	196778	193228

Cascade No.1 offers reduction of 7% in total pressure loss, needs 1 airfoil less than the VKI cascade, and generates about 1% higher total loading. Cascade No.3 offers reduction of 5% in total pressure loss, need 1 more airfoil than the VKI cascade, and generates about 6% higher total loading. Cascade No.6 offers reduction of 7% in total pressure loss, need the same number of airfoils as the VKI cascade, and generates about 4% higher total loading. The cascade No.1 may be the best compromise among three optimized cascades for many turbomachinery designs.

This means that it is possible to design turbomachinery blade rows that will have simultaneously lower total pressure loss, higher total loading, and fewer blades while preserving some of the same features of the original blade rows (inlet and exit flow angles, total mass flow rate, blade cross-section area, and trailing edge radius). Actual difference in the geometric shapes of the original VKI airfoil and the three representative optimized cascades is clearly visible (Fig. 3).

The three optimized cascade airfoil geometries are quite similar. This is because we have 4 equality constraints and 3 objectives to satisfy. Consequently, the feasible domain of design variables (the ranges of design variables that satisfy the specified constraints) is very small⁶ and the geometries and pressure fields (Figs. 7-10) for the three best optimized solutions are very similar. It appears that both the passage shock and the trailing edge shock are weaker in the optimized configurations as compared to the original VKI finite cascade.

We used 600 points on the airfoil surface that typically resulted in a grid of approximately 20000 triangles. Clustering the grid especially around trailing edge and closer to the airfoil surface can influence the results especially if there are strong trailing edge shocks like in this supersonic exit cascade case. The results achieved can also be influenced by the choice of the turbulence model or a transition point location. Thus, the role of the designer is to use a proven and robust flow-field analysis code and specify meaningful ranges of the design variables, the multiple objective functions, and the constraints. Finally, the designer ultimately must choose the best compromise solution among the optimized solutions that form the Pareto front.

All computations were performed on our 32 node distributed memory parallel computer with 400 MHz Pentium II processors and a total of 8GB RAM. Each call to IOSO consumed a negligible fraction of computing time compared to each call to the flow-field analysis code which consumed about 15 minutes on a single processor. The overall computing time for this test case on our parallel machine consumed approximately 50 hours. Although the optimization problem seemed relatively easy (only three objectives, 18 design variables and five constraints), it consumed a total of 5611 analysis calls to the 2-D flow-field analysis code in order to find enough points in the feasible region having relative errors in equality constraints less than one percent.

In other words, the size of the feasible domain in the design variable space was extremely small since it was reduced by numerous constraints. Furthermore, the feasible domain proved to have a very complex topology thus making this multi-objective constrained optimization problem a very challenging test case for any optimizer.

The original VKI cascade already had a very high efficiency since it was designed using an inverse shape design method. The number of airfoils that we used in the original finite VKI cascade was already extremely small.

VII. Conclusions

Using a robust Navier-Stokes flow-field analysis code, a flexible geometric parameterization formulation, a reliable grid generation code, and a multi-objective stochastic optimization algorithm with a number of user-specified constraints, it was demonstrated that it is possible to automatically design airfoil cascade configurations that will be more efficient and have fewer airfoils than the existing good cascades. This multi-objective design optimization methodology can be easily extended to 3-D blade row configurations.

Acknowledgments

The authors would like to express their gratitude for the National Science Foundation Grants DMI-9522854 and DMI-9700040 monitored by Dr. George A. Hazelrigg, the NASA Lewis Research Center Grant NAG3-1995 facilitated by Dr. John K. Lytle and monitored by Dr. Kestutis Civinskas, Lawrence Livermore subcontract B506167 facilitated by Dr. J. Ray Smith and monitored by Dr. Lou Ann Tung, and for the Lockheed Martin Skunk Works grant facilitated by Mr. Thomas Oatway and monitored by Mr. Atherton Carty.

References

¹Goel, S., Cofer, J. I. and Singh, H., "Turbine Airfoil Design Optimization", ASME paper 96-GT-158, ASME IGTI, June 13-16, 1996, Birmingham, United Kingdom.

²Trigg, M. A., Tubby, G. R. and Sheard, A. G., "Automatic Genetic Optimization Approach to 2D Blade Profile Design for Steam Turbines", ASME paper 97-GT-392, ASME Turbo Expo97, Orlando, Florida, U.S.A., June 1997.

³Li, J., Feng, Z. Chang, J.-Z. and Shen, Z., "Aerodynamic Optimum Design of Transonic Turbine Cascades Using Genetic Algorithms", *Journal of Thermal Sciences*, Vol. 6, No. 2, 1997, pp. 111-116.

⁴Giannakoglou, K. C., "A Design Method for Turbine Blades Using Genetic Algorithms on Parallel Computers," Fourth ECCOMAS Computational Fluid Dynamics Conference, Athens, Greece, September 7-11, 1998 (editors: K. Papailiou, D. Tsahalis, J. Periaux, C. Hirsch and M. Pandolfi), John Wiley & Sons, New York, Vol. 1, Part 1, 1998, pp. 354-359.

⁵Dulikravich, G. S., Martin, T. J., Dennis, B. H. and Foster, N. F., "Multidisciplinary Hybrid Constrained GA Optimization", Invited lecture, Chapter 12 in EUROGEN'99 - *Evolutionary Algorithms in Engineering and Computer Science: Recent Advances and Industrial Applications*, (editors: K. Miettinen, M. M. Makela, P. Neittaanmaki and J. Periaux), John Wiley & Sons, Ltd., Jyväskylä, Finland, May 30 - June 3, 1999, pp. 231-260.

⁶Dennis, B. H., Dulikravich, G. S. and Han, Z.-X., "Constrained Optimization of Turbomachinery Airfoil Cascade Shapes Using a Navier-Stokes Solver and a Genetic/SQP Algorithm", ASME paper 99-GT-441, ASME Turbo Expo99, Indianapolis, Indiana, U.S.A., June 7-10, 1999; also to appear in *AIAA Journal of Propulsion and Power*, 2000.

⁷Petrovic, M. V., Dulikravich, G. S. and Martin, T. J., "Maximizing Multistage Turbine Efficiency by Optimizing Hub and Shroud Shapes and Inlet and Exit Conditions of Each Blade Row," ASME paper 99-GT-071, ASME Turbo Expo, Indianapolis, Indiana, U.S.A., June 7-10, 1999; also in *International Journal of Turbo & Jet Engines*, 2000.

⁸Petrovic, M. V., Dulikravich, G. S. and Martin, T. J., "Optimization of Multistage Turbines Using a Through-flow Code," ASME paper 2000-GT-0521, ASME Turbo-Expo-2000, Munich, Germany, May 8-11, 2000.

⁹Goel, S. and Hajela, P., "Turbine Airfoil Design Using Reinforcement Learning Based Optimization", AIAA paper 98-4774, 1998.

¹⁰Poloni, C., Pediroda, V., Onesti, L. and Giurgevich, A., "Hybridisation of MultiObjective Genetic Algorithm, Neural Networks and Classical Optimizer for Complex Design Problems in Fluid Dynamics", *Computational Methods in Mechanics and Engineering*, June 1999.

¹¹Egorov, I. N., "Indirect Optimization Method on the Basis of Self-Organization", Curtin University of Technology, Perth, Australia, *Optimization Techniques and Applications (ICOTA '98)*, Vol. 2, 1998, pp. 683-691.

¹²Egorov, I. N., Kretinin, G. V., Leshchenko, I. A., Kostiuk, S. S., "The Methodology of Stochastic Optimization of Parameters and Control Laws for the Aircraft Gas-Turbine Engines Flow Passage Components", ASME paper 99-GT-227, ASME Turbo Expo, Indianapolis, Indiana, U.S.A., June 7-10, 1999.

¹³Pritchard, L. J., "An Eleven Parameter Axial Turbine Aerofoil Geometry Model", ASME paper 85-GT-219, 1985.

¹⁴Han, Z.-X., Fang, R. and Liu, Z.-J., "2-D Flowfields Calculation with Multi-Unstructured Grids", *Journal of Aerospace Power*, No. 3, 1998 (in Chinese).

¹⁵Shewchuk, R. J., "Triangle: Engineering a 2D Quality Mesh Generator and Delaunay Triangulator", 1st Workshop on Applied Computational Geometry, ACM, Philadelphia, PA, May 1996, pp. 124-133.

¹⁶Jameson, A. and Mavriplis, D., "Finite Volume Solution of the Two-Dimensional Euler Equations on a Regular Triangular Mesh", *AIAA Journal*, Vol. 24, No. 4, 1986, pp. 611-618.

¹⁷Morrison, J., "Flux Difference Split Scheme for Turbulent Transport Equations", AIAA Paper 90-5251, 1990.

¹⁸Frink, N. T., "Recent Progress Toward a Three-Dimensional Unstructured Navier-Stokes Flow Solver", AIAA Paper 94-0061, 1994.

¹⁹Roe, P. L., "Characteristic Based Schemes for the Euler Equations", *Annual Review of Fluid Mechanics*, Vol. 18, 1986, pp.337-365.

²⁰Sieverding, C. H., "Test Case E/CA-8 Transonic Turbine Cascade", in AGARD AR 275: "Test Cases for Computation of Internal Flows in Aero Engine Components", (editor: Fottner, L.), 1990, pp. 139-151.

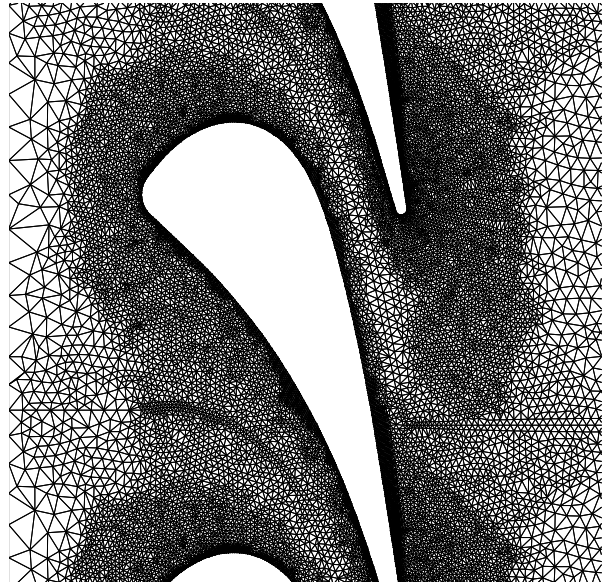


Fig. 1 A typical non-structured computational grid used.

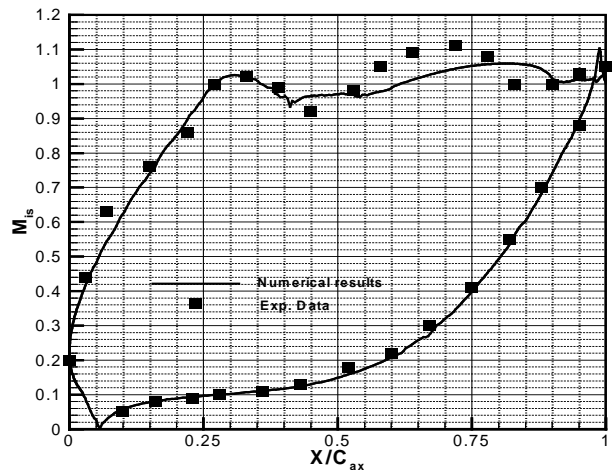


Fig. 2 Surface isentropic Mach number distribution on the original VKI turbine airfoil cascade with sonic exit flow condition: comparison of experimental data and numerical results obtained using our Navier-Stokes flow-field analysis code.

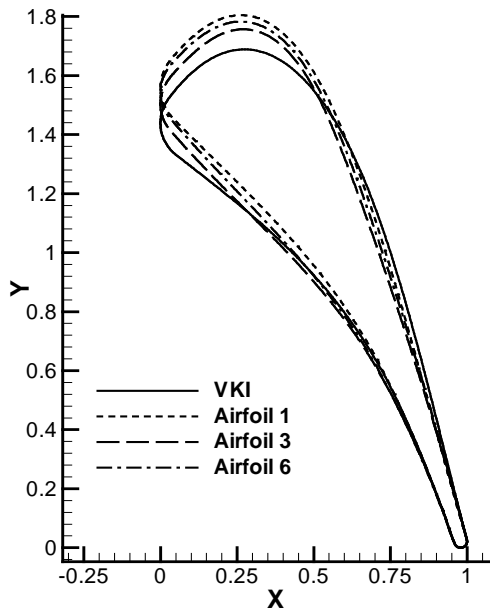


Fig. 3: Comparison of three optimized airfoil cascades against the original VKI airfoil cascade.

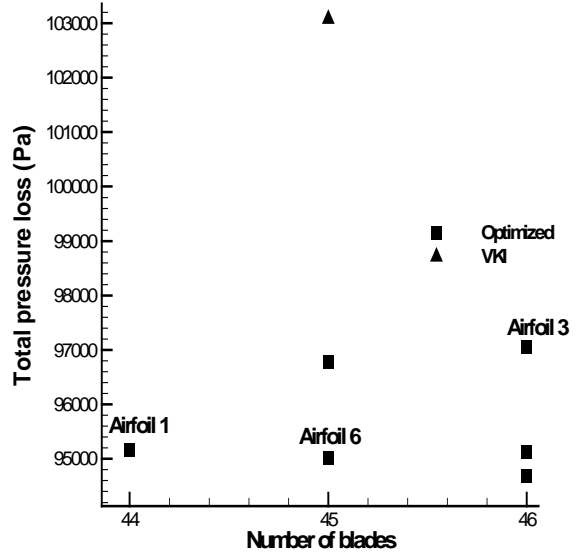


Fig. 5: Comparison of total pressure loss generated versus number of airfoils for cascades of optimized airfoils and for the original VKI airfoil cascade.

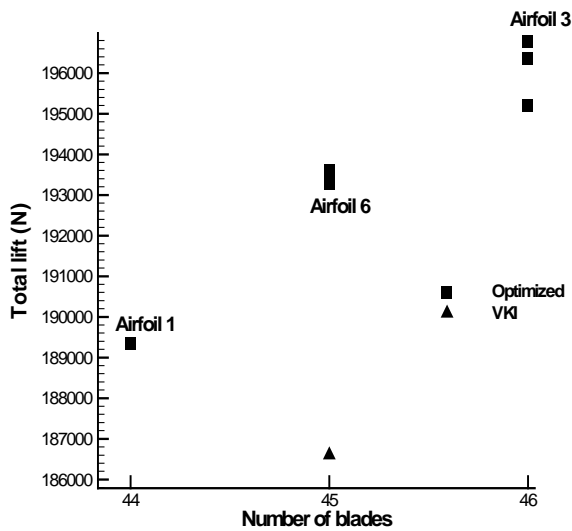


Fig. 4: Comparison of total lift produced versus number of airfoils for optimized airfoil cascades and the VKI airfoil cascade.

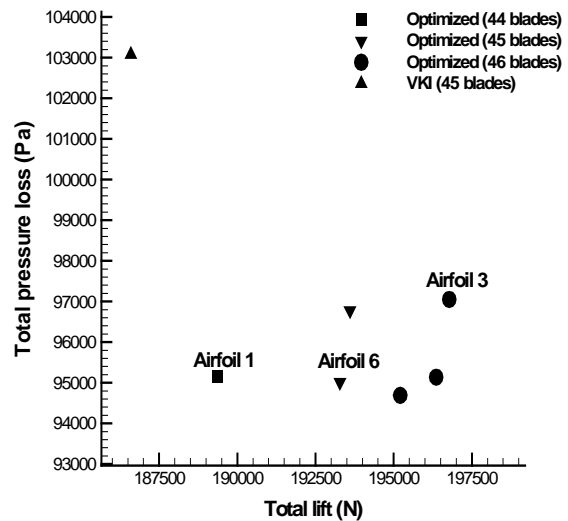


Fig. 6: Comparison of total pressure loss generated versus total loading produced for various numbers of airfoils for optimized airfoil cascades and the VKI airfoil cascade.

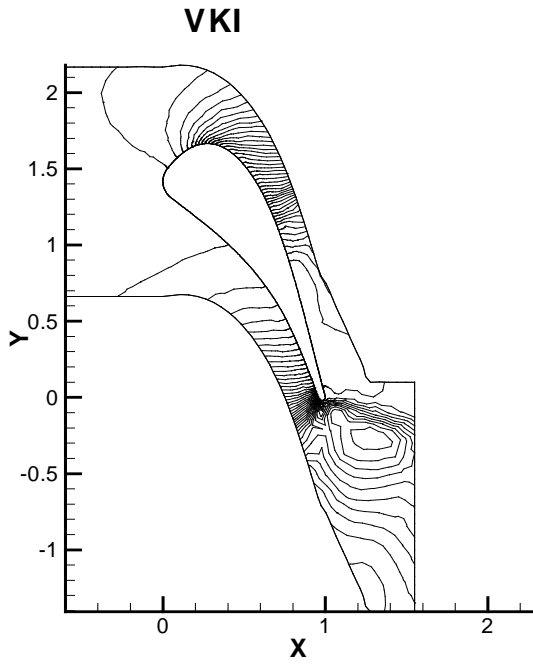


Fig. 7: Static pressure field for VKI airfoil cascade.

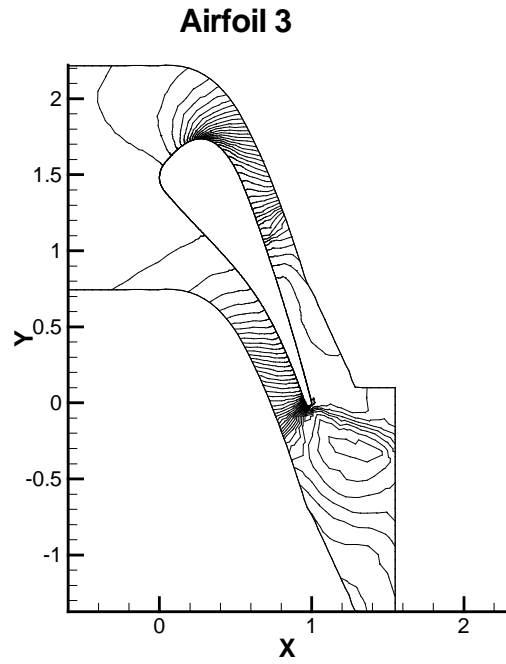


Fig. 9: Static pressure field for optimized cascade No.3.

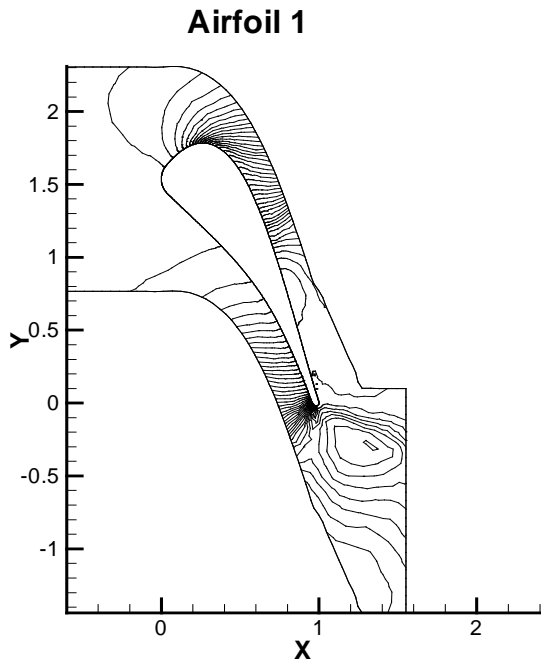


Fig. 8: Static pressure field for optimized cascade No.1.

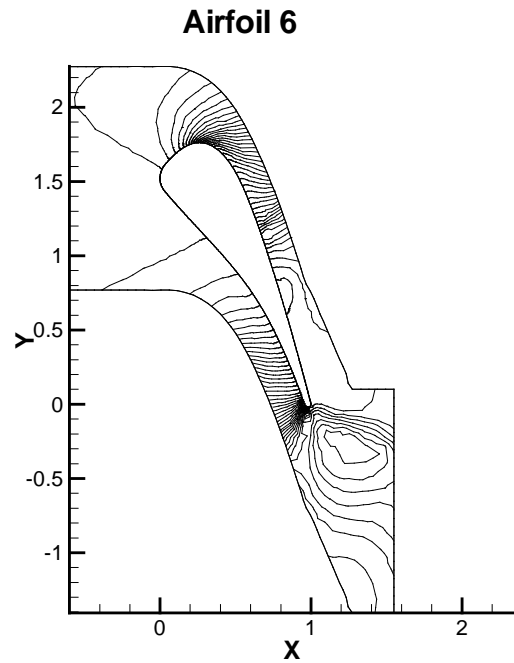


Fig. 10: Static pressure field for optimized cascade No.6.